NEUROSCIENCE

Visualizing 3D imagery by mouth using candy-like models

Katelyn M. Baumer, Juan J. Lopez, Surabi V. Naidu, Sanjana Rajendran, Miguel A. Iglesias, Kathleen M. Carleton, Cheyanne J. Eisenmann, Lillian R. Carter, Bryan F. Shaw*

Handheld models help students visualize three-dimensional (3D) objects, especially students with blindness who use large 3D models to visualize imagery by hand. The mouth has finer tactile sensors than hand, which could improve visualization using microscopic models that are portable, inexpensive, and disposable. The mouth remains unused in tactile learning. Here, we created bite-size 3D models of protein molecules from "gummy bear" gelatin or nontoxic resin. Models were made as small as rice grain and could be coded with flavor and packaged like candy. Mouth, hands, and eyesight were tested at identifying specific structures. Students recognized structures by mouth at 85.59% accuracy, similar to recognition by eyesight using computer animation. Recall accuracy of structures was higher by mouth than hand for 40.91% of students, equal for 31.82%, and lower for 27.27%. The convenient use of entire packs of tiny, cheap, portable models can make 3D imagery more accessible to students.

INTRODUCTION

Approximately 36 million people have blindness, including 1 million children ([1, 2]). An additional 216 million people experience moderate to severe visual impairment ([1]). Students with blindness or low vision (BLV) face challenges in science, technology, engineering, and math (STEM) ([3–5]). Besides barriers imposed by limited assistive technology ([6]), students with blindness face bias by educators and peers ([7, 8]). This bias can erode a student's sense of belonging ([9, 10]), make science appear too challenging to pursue ([11]), and inhibit social groups that promote interest ([12]). New assistive technology might increase inclusion and decrease bias ([13]).

The importance of visual stimuli in early conceptual development requires a multisensory approach to teaching students with BLV ([14, 15]). Braille, tactile graphics, tactile models, text-to-audio, and other assistive technologies have improved learning in the classroom and laboratory ([16–19]). However, the growing use of three-dimensional (3D) imagery in STEM education—especially online learning—is requiring visualization of greater numbers of 3D graphics ([20–22]). Even an "old" introductory textbook of biochemistry contains ~1100 illustrations, including 3D depictions of proteins with thousands of atoms (e.g., hemoglobin: $C_{2952}H_{4664}O_{832}N_{812}Fe_4$) ([23]).

For students with blindness to accurately visualize a 3D image or system—for example, an atomic structure of a folded protein—each image must be converted into a 3D model for tactile visualization by fingertip, i.e., visualization by manual stereognosis ([15, 24]). Conventional models are inconvenient to have in large pedagogical sets because they are typically large (centimeter to meter in scale) and can be expensive ([16]). Consequently, students do not receive one model for each image in a textbook. Much of the imagery in STEM—the spectacular imagery that sparks early interest—is inaccessible to students with blindness. Methods are needed to enable inexpensive, convenient visualization of 10^2 models (images) per student, per course.

We hypothesize that tactile visualization can be improved by using millimeter-scale models that are visualized by the tongue and lips, i.e., oral stereognosis ([25–29]), as well as hands. The tactile sensitivity

of the mouth is greater than fingertip ([30–32]). For example, the tactile resolution of fingers, lips, and tongue has been measured to be 0.94 mm (fingers), 0.51 mm (lips), and 0.58 mm (tongue) ([31]). The tongue can also distinguish sub-micrometer differences in surface roughness ([30, 33]), and its taste buds could be used to read information encoded by flavor. Despite these advantages, the use of oral stereognosis in education is unreported ([34]).

Brain imaging suggests that feelings of touch (somatosensory input) from our tongue, lips, and teeth converge across the primary somatosensory cortex ([35, 36]) to produce a "conscious mouth image" ([28]). The utility of the tongue in painting this mental picture of the oral cavity—and objects in it—is based on its high innervation density and octopus-like rheology ([37]). Our tongue is a muscular hydrostat (similar to an octopus arm) with muscle fibers parallel and transverse to the long axis, which allows elongation, shortening, and bending ([38, 39]). The tongue can conform to surface features that would be untouched by a fingertip ([40, 41]). This pliability can explain oral-haptic illusions, where surface features are perceived to be larger when sensed by the tongue compared to fingertips ([40, 41]).

We do not hypothesize (or expect) that persons with blindness will have enhanced oral tactile acuity. Oral tactile spatial acuity is unaffected by blindness ([29, 42]). Tactile spatial acuity of fingertips is reportedly enhanced by blindness ([43, 44]). However, a statistical analysis of previous measurements ([42–52]) of tactile acuity of fingertips in persons with and without blindness (M) yields a value of $\Delta M_{\text{sight-blind}} = 0.100 \pm 0.820$ mm ($n = 582$, $P = 0.0007$; table S1). While enhancement in tactile spatial acuity per blindness is statistically significant, it is highly variable and its effects are practically negligible to the current study (table S1).

RESULTS AND DISCUSSION

This study was approved by an Institutional Review Board at Baylor University. The goals of this study were to create smaller, more practical tactile models of 3D imagery—that fit in the mouth—and compare the utility of hand, mouth, and eyesight in visualization. These models are intended for use by all students, with or without visual impairment. 3D printing and food-safe silicone molding

Department of Chemistry and Biochemistry, Baylor University, Waco, TX, USA.
*Corresponding author. Email: bryan_shaw@baylor.edu

were used to fabricate millimeter-scale models (edible and nonedible) of atomic structures of folded proteins (Fig. 1). The models have micrometer-scale surface features depicting electron clouds (i.e., van der Waals surfaces). Folded proteins were chosen because their structures are some of the most numerous, complex, high-resolution 3D images presented throughout STEM. Moreover, the study of protein function requires perception of subtle changes in their 3D structure and shape. Structure equals function is a central dogma in biochemistry.

Converting molecular graphics into tiny 3D models

Space-filling models of globular proteins were fabricated to be exact replicas of x-ray crystal structures deposited by structural biologists into the Protein Data Bank (PDB). Models were made of either nonedible (but biocompatible) surgical resin (Fig. 1, A and B) or firm edible gelatin, i.e., "gummy bear" material (Fig. 1C). Nine different protein structures were modeled (Fig. 1, B and C): Cu, Zn superoxide dismutase 1 (SOD1), myoglobin (Mb), carbonic anhydrase II (CA II), apo-hexokinase (apo-HK), holo-hexokinase (holo-HK), apo-calmodulin (apo-CaM), holo-calmodulin (holo-CaM), apo-maltose binding protein (apo-MBP), and holo-maltose binding protein (holo-MBP). Note that six of the nine proteins include pairs of allosteric conformers, that is, two different shapes of the same molecule ("apo" or "holo" shapes of either CaM, MBP, or HK). The apo and holo conformers of CaM, MBP, or HK differ in structure due to the binding of a metal ion or carbohydrate (Fig. 1, A to C).

We fabricated models in two sizes, denoted "small" and "smaller." Small models (Fig. 1, B, top, and C) are the size of a peanut (~5 to 20 mm in diameter). Smaller models (Fig. 1, A and B, bottom) are the size of rice grain (~2 to 10 mm in diameter), and both easily fit into the mouth. Nonedible models were printed with an eyelet for the attachment of a safety loop (e.g., dental floss; Fig. 1D). This lanyard can be held by the student to prevent swallowing or used to attach a label. Smaller models were fabricated to minimize cost and maximize convenience (ease of storage and transport) when dozens or hundreds of models would be needed to accompany each 3D image in a learning module. For example, smaller models can be easily arrayed onto an index card with laminate packaging (Fig. 1E) or stored in small containers, like candy (Fig. 1, F and G). Edible gelatin models were only made in the small size, as the smaller gelatin CaM model—with its single α-helical neck—would frequently break during use.

Information about edible or nonedible/biocompatible models could be encoded with flavor (Fig. 1, C and F). Even smaller nonedible/biocompatible models could be coated with flavors (and food coloring) without lowering their structural resolution (Fig. 1F). As a demonstration, we filled a partitioned box of "Nerds" candy with models coded in grape and orange (Fig. 1F).
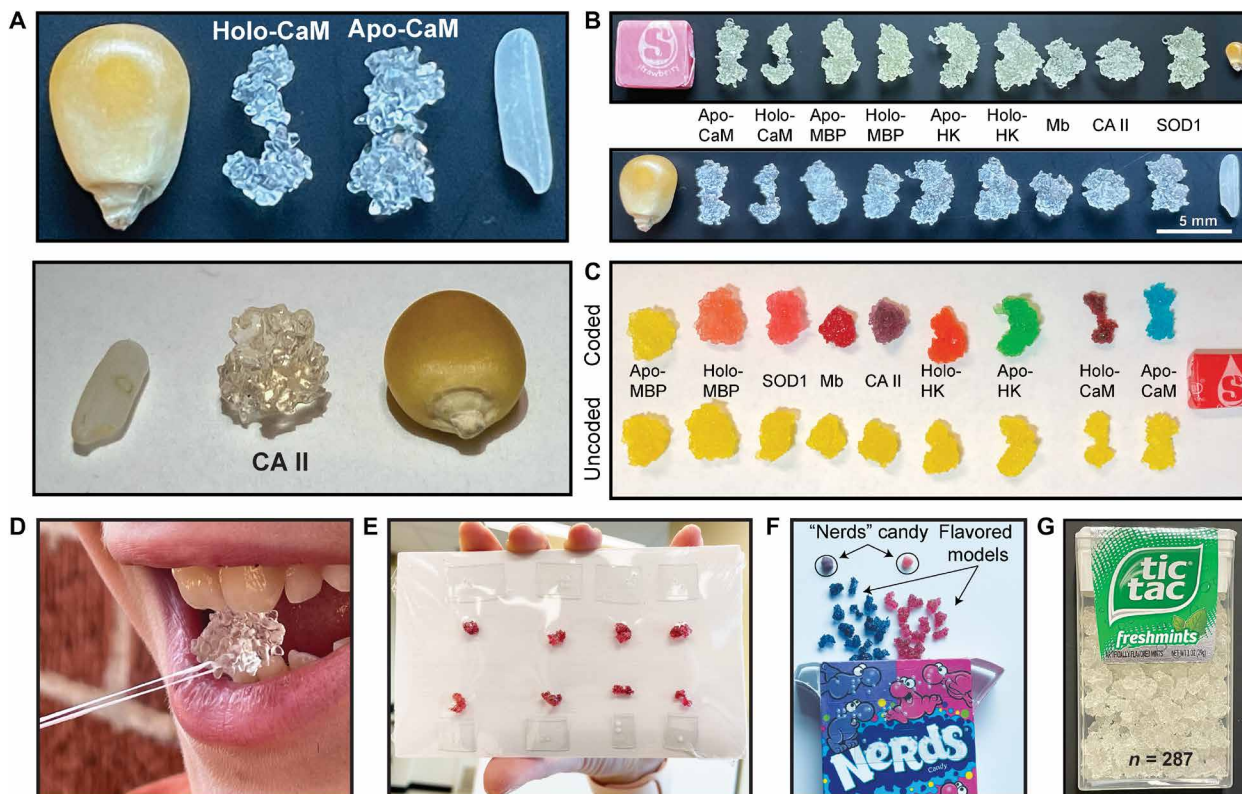
Fig. 1. "Small" and "smaller" molecular models: Highly portable and encodable with flavor. (**A**) Smaller nonedible 3D-printed models of calmodulin (CaM) and carbonic anhydrase II (CA II) are comparable in size to a popcorn kernel or grain of rice. Array of protein models fabricated and tested in this study from (**B**) biocompatible resin (top: small size; bottom: smaller size) or (**C**) gelatin (flavor-coded or uncoded). (**D**) Small nonedible model with a safety lanyard threaded through the integral eyelet. (**E** to **G**) Smaller nonedible models can be coded with flavor and transported in high volume. (E) Shrink-wrapped array onto a standard index card and (F and G) packed into common containers of candy (shown for demonstration purposes). Photo credit: Jordan C. Koone, Baylor University; Bryan F. Shaw, Baylor University; and Elizabeth Shaw.

Gelatin models (Fig. 1C) were fabricated by injecting hot gelatin into a food-grade silicone mold of each protein structure (Fig. 2). The preparation of the silicone mold (Fig. 2)—bearing the debossed protein structure—is simple and inexpensive. Nonedible models were 3D-printed in a food-safe environment using a biocompatible, autoclavable surgical resin, followed by sterilization in a food-grade autoclave.

Each edible or nonedible model accurately depicted the atomic structure of the protein, with micrometer-scale contours depicting van der Waals surfaces (Fig. 3). The bulbar topology of the van der Waals surfaces ranged from approximately 700 to 3000 µm (peak to peak) for small models and 200 to 1000 µm for smaller models. Intramolecular contacts could be accurately modeled in the gelatin model. For example, a salt bridge between the guanidinium and carboxylic functional groups in CaM is accurately modeled (Fig. 3, C and D).

Nonedible biocompatible models differ from the gelatin models in one structural respect: They contain an eyelet for the attachment of a safety lanyard (e.g., a loop of thread or dental floss) (Fig. 3D).

### Recognizing tiny molecular models by hand or mouth

In this study, identical testing was carried out on edible gelatin models and nonedible 3D-printed models. To prevent students from seeing models during tactile testing, each student was blindfolded regardless of visual acuity. At this proof-of-concept stage, we chose to not experiment upon or test children or students with BLV because they may represent a vulnerable population continually sought for research (53). Rather, we experiment on nonvulnerable model subjects (i.e., sighted students). Sighted students are adequate model subjects for testing because (i) oral tactile spatial acuity is not generally affected by blindness (29), (ii) effects of blindness on manual tactile spatial acuity are below the resolution limit of micromodels (i.e., $\Delta M_{\text{sight-blind}} = 0.100 \pm 0.820$ mm; table S1), (iii) short-term visual deprivation (blindfolding) does not enhance tactile spatial acuity (54), and (iv) tactile micromodels are intended for sighted students too. This study did include a single survivor of bilateral retinoblastoma who has significant blindness. This technology was designed specifically for this survivor, and they were consulted during its development.

Each college-age student who participated in tests of oral and manual stereognosis (n = 281 students) was first given one small or smaller model of an allosteric protein to tactilely sense with their hands. This model is referred to as the "study" model (Fig. 4). Each student was then given a series of eight protein models (including two examples of the study model) to tactilely sense by hand. After each model was handled, the student was asked to answer "yes" or "no" to the question: "Is this model identical to the first (study) model that we gave you?" Tests scores were calculated from the quotient of correct answers and total questions. For assessments of oral stereognosis, the same test format was used on the same student, using the same models. Here, students had the same study model placed into their oral cavity (while blindfolded). The same series of different models were then placed in their mouth (as in the manual test), and they were asked to answer yes or no to the question: "Is this model identical to the first (study) model that we gave you?" In total, 16 tests of oral and manual stereognosis were performed on each college-age student (n_{total} = 4496 tests).

Comparative accuracy of structure recall by hand and mouth

Before testing oral and manual stereognosis on college-age students, we first performed pilot tests of oral and manual stereognosis on a survivor of bilateral retinoblastoma (Fig. 5). This student (age 10 years) has partial vision in one eye, but his other eye was removed during infancy. He is the first person on whom we tested this technology, and for whom it was initially developed (he is the son of the corresponding author of this study). Each answer given by this student is shown (Fig. 5, A and B). We do not group his scores in the aggregate data with other students but report his results as an internal case study, as he was tested on an expanded number of models. He was blindfolded during testing.
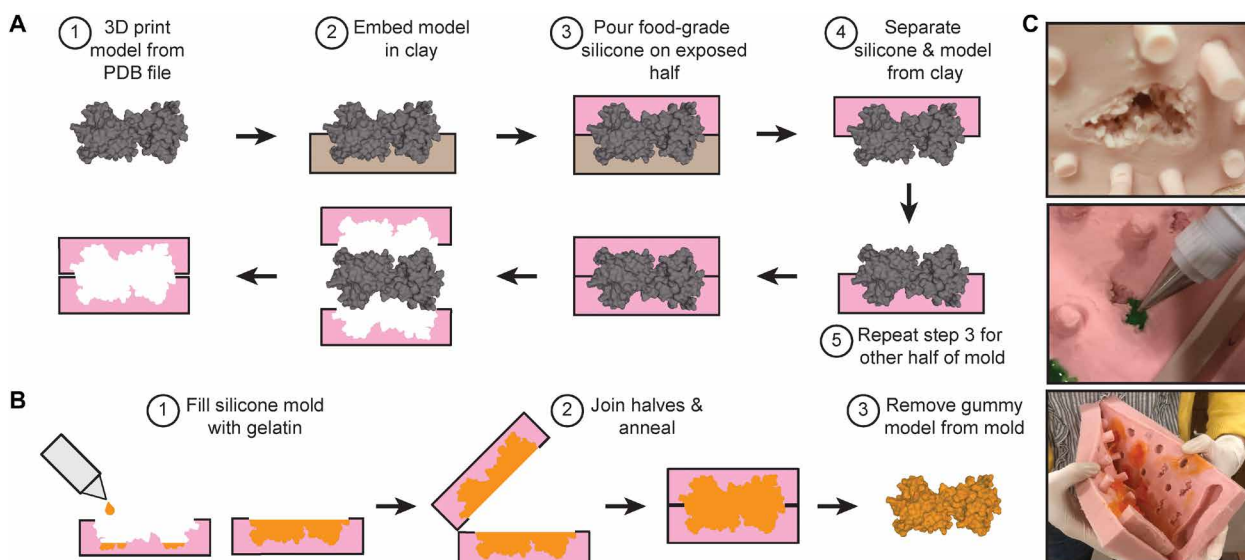
Fig. 2. Fabrication of reusable silicone mold for producing edible models of 3D imagery. (**A**) Fabrication of food-grade silicone mold from 3D-printed space-filling model of a folded protein. The structure of the protein is derived from the public PDB. (**B**) Fabrication of edible mouth models by injection of edible material into silicone mold. (**C**) Silicone molds (top, middle, and bottom). Injection of gelatin (middle) and separation of molds after curing of gelatin (bottom). Photo credit: Bryan F. Shaw, Baylor University.
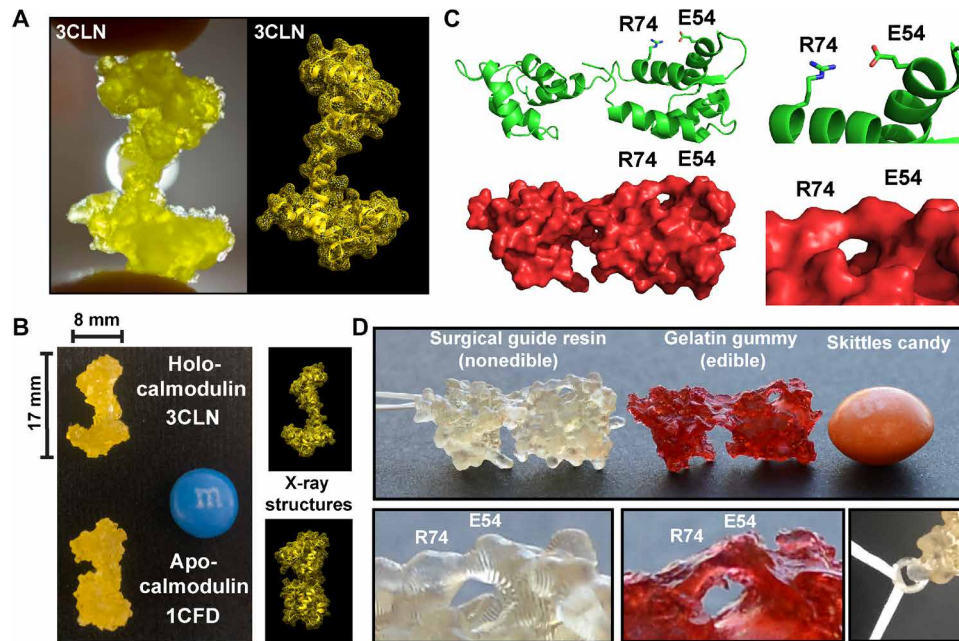
Fig. 3. Atomic accuracy and safety of edible and nonedible miniature models. (**A**) Comparison of small gelatin model (left) and x-ray crystal structure (right) of holo-CaM (PDB: 3CLN). Note that the single α-helical neck is maintained in the gelatin model. (**B**) Comparison of gummy models of holo-CaM and apo-CaM (left) and computer renderings (right); PDB codes: 3CLN and 1CFD. (**C**) X-ray crystal structures of apo-CaM highlighting salt bridge between arginine-74 and glutamate-54. (**D**) The salt bridge is accurately rendered in the small gelatin model (red, right) and in the 3D-printed model (clear, left). The small 3D-printed model contains an eyelet to attach a safety lanyard. Photo credit: Bryan F. Shaw, Baylor University.

In tests using small gelatin models, this student used oral stereognosis to correctly answer 31 of 40 questions (column "O"; Fig. 5A), for a recall accuracy of 77.50%. When the test was repeated (weeks later), the student correctly answered 15 of 40 questions using manual stereognosis (column "M"; Fig. 5A), for a recall accuracy of 37.50%. A smaller battery of tests, with fewer test proteins, produced similar results: 16 of 20 questions correctly answered using oral stereognosis (80% accuracy) and 8 of 20 using manual stereognosis (40% accuracy).

Comparisons of college-age students' abilities to use oral or manual stereognosis to recall small and smaller models revealed that oral and manual tactile recall were equivalent for many students (Fig. 4, A and B). For example, 39.86% of college students earned identical scores on oral and manual tests involving small and smaller models (Fig. 4C and Table 1). Raw test scores for each participant can be found in table S2. Recall accuracy varied per size of model (Fig. 4D and Table 1), as discussed below. In total, for 28.11% of students tested, manual stereognosis was superior to oral stereognosis. For 32.03% of students tested, oral stereognosis was superior to manual stereognosis (Fig. 4C and Table 1). Scores of superior performance by either manual or oral stereognosis were, on average, 18.71% higher than the inferior score by that student (table S2). Accuracy ranged from 25.0 to 100.0% for both manual and oral stereognosis (table S2). There were no observable differences in recall between biological sex ($P = 0.0523$, manual; $P = 0.6375$, oral) (table S2).

In total, small and smaller structures were recalled at $85.59 \pm 14.65\%$ accuracy by oral stereognosis and at $84.83 \pm 15.14\%$ accuracy by manual stereognosis ($P = 0.5477$) (Table 1). We did not investigate why some students used oral stereognosis more effectively than others. However, previous studies suggest that pure lingual tactile sensitivity correlates with fungiform papillae (taste bud) density (55).

We hypothesized that the recall accuracy of oral stereognosis might increase further over manual stereognosis as models decrease in size. A larger percentage of students (40.91% of students) given smaller models had superior performance with oral than manual stereognosis, compared to only 20.51% of students having superior oral recall of small models ($P = 0.0046$) (Fig. 4C and Table 1). On average, however, smaller models were identified (by college-age students) with statistically similar accuracy to small models (Fig. 4D and Table 1).

Ninety percent of tests of college-age students in this study were carried out with nonedible models: 249 students were tested with nonedible models (3984 nonedible tests in total). Only 32 students were tested with edible models (8 oral tests, 8 manual tests; 512 tests in total). Fabricating edible models is more labor intensive. The structural accuracy of edible models was comparable to the x-ray crystal structure (Fig. 3). Gelatin models were correctly recalled at rates comparable to recall of nonedible models of similar size (Fig. 4D) ($P = 0.1558$, manual; $P = 0.0235$, oral). This similarity is due, we presume, to the maintaining of shape of the gelatin models after being inside a student's mouth for 5 min (Fig. 5C).

To test how adaptable primary school students are to oral tactile testing, we tested small nonedible models on children in the fourth and fifth grades. For these tests, all models contained a safety lanyard (Fig. 3D). Here, 186 manual and oral tests of stereognosis were carried out on 31 grade school students. We keep scores of grade school students separate from the college-age students because the size of the test was truncated from eight to three models but was otherwise carried out in identical format. The relative recall accuracy
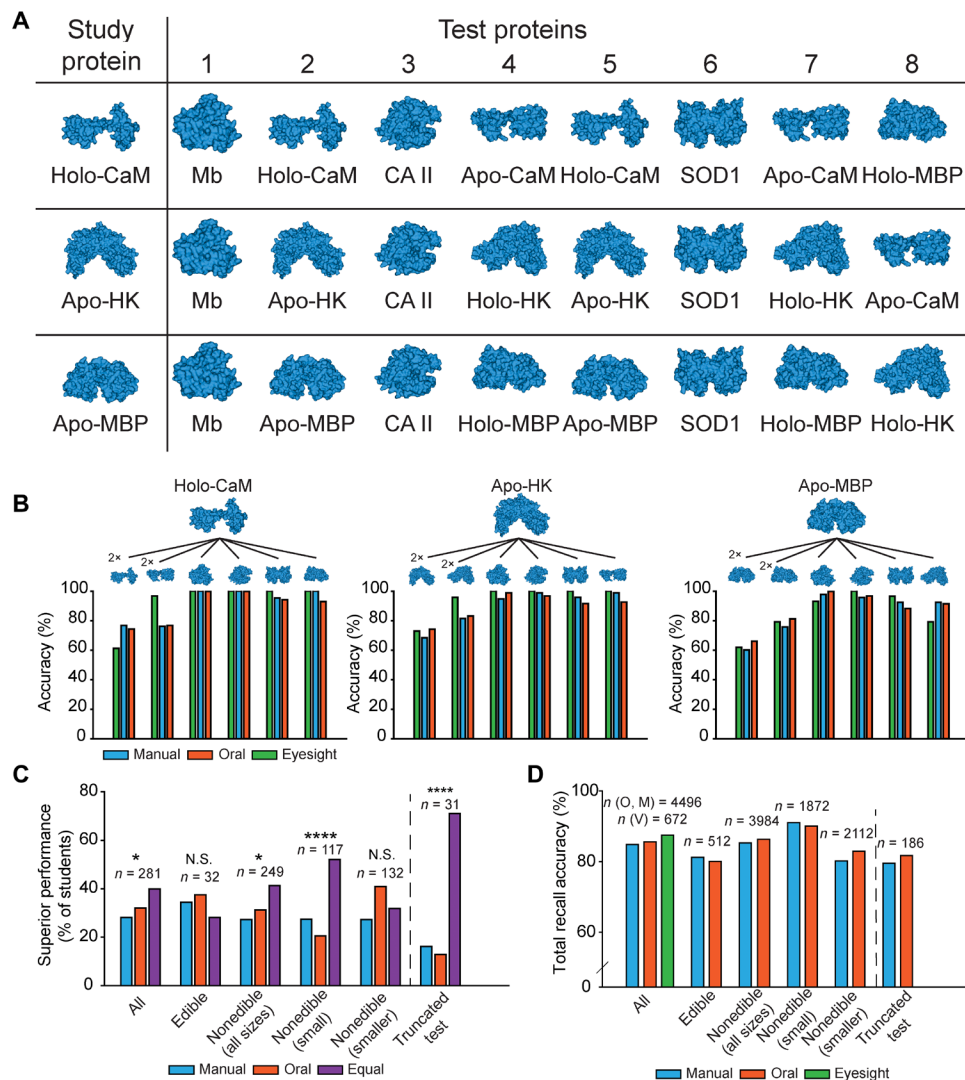
Fig. 4. Student performance at recognizing 3D models (edible and nonedible) by oral tactile sensing or hand (manual) tactile sensing versus eyesight of a larger moving image (5261 tests performed on 396 students). (**A**) Testing format used throughout this study (PDB codes for models are listed in Materials and Methods). Each row represents a different test variation. (**B**) Recall accuracy in each test variation. Identical structures and conformers were tested twice as many times as other proteins (denoted by "2×"). (**C**) Percentage of college students in this study who exhibited higher accuracy of recognition of structures by manual/hand tactile sensing (M), oral tactile sensing (O), or demonstrated equal accuracy with oral and manual sensing; n, number of students tested. Truncated test group refers to 186 tests conducted on 31 grade school students (using only three models per student per each oral or manual test). Statistical significance was determined using a χ^2 analysis: N.S., not significant; *$P < 0.05$; **$P < 0.01$; ***$P < 0.001$; ****$P < 0.0001$. (**D**) Total recall accuracy for manual (M) and oral (O) sensing and eyesight (V) in all tests; n, total number of tests performed in each category.

of oral and manual stereognosis was similar to college-age students (Fig. 4D and Table 1). However, a larger percentage of fourth and fifth graders showed equal accuracy in oral and manual stereognosis, compared to college-age students (Fig. 4C and Table 1).

Quantifying limits of shape discrimination by hand and mouth

The geometric dissimilarity of two model protein structures was quantified using Eq. 1. Briefly, we calculated the product of the ratio of each model's surface area, volume, and cubicity (i.e., 1,000,000 x, y, and z coordinates on each surface). Dissimilarity scores ranged from 4.380 to 36.307, where a score of zero corresponded to two identical structures (Fig. 6A). The structures that were most often

confused by students (orally or manually) were those with the most similar geometry/topology (lowest score), i.e., allosteric conformers (Fig. 6, B to D). For example, holo-MBP and apo-MBP were the two structures having the most similar shape (score = 4.380). Apo-MBP was misidentified by mouth as being holo-MBP protein in 18.82% of tests (involving small and smaller models) (Fig. 6, B to D). Apo-MBP was misidentified by hands in 24.19% of tests. The relationship between geometric similarity and recall accuracy reveals two points: (i) Structures with very high dissimilarity were never incorrectly recalled by mouth or hand and (ii) structures with identical shapes were not always correctly recalled by mouth or hand. Identical structures were correctly recalled in only 72% of tests by mouth and 68% by hand (Fig. 6, C and D).
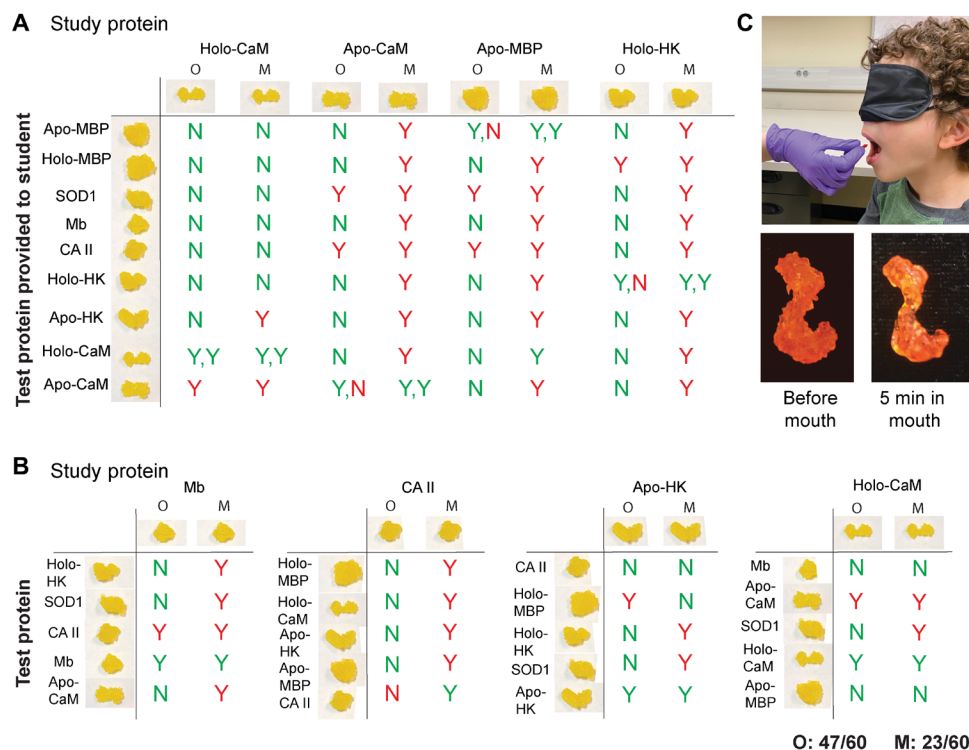
Fig. 5. Example tests of oral tactile sensing (O) and manual/hand tactile sensing (M) of small gelatin models on a visually impaired survivor of bilateral retinoblastoma. (**A**) Correct answers to the question: "Is this the study protein" are coded green; incorrect answers are coded red; yes = Y; no = N. (**B**) Similar tests as in (A) but using a smaller number of proteins. The ratio of correct answers to total questions from tests in (A) and (B) is given in the lower right corner. (**C**) The gross morphology of the small gelatin model of holo-CaM was maintained after 5 min in the student's mouth. Photo credit: Bryan F. Shaw, Baylor University.

Comparing recall by eyesight to recall by hand or mouth

We assessed the ability of a separate set of college-age students (n = 84 students) to visually identify and recall large images of protein structures on their computer screen, without the assistance of physical models. These recall tests by eyesight were performed on students who had not participated in tactile tests with models and who did not have visual impairments. The same protein structures were used as in oral and manual tests (i.e., eight tests per student). We did not reduce the size of the molecular images to the millimeter scale of the small or smaller models. Rather, we allowed the students to use eyesight to visualize graphics at the conventional sizes used by biochemistry students or structural biologists (i.e., centimeter scale). In total, 672 tests of recall by eyesight were performed.

Structures were recalled by eyesight with similar accuracy to tactile tests, i.e., 87.50 ± 13.58% accuracy by eyesight, compared to 84.83 ± 15.14% and 85.59 ± 14.65% for manual and oral stereognosis (Fig. 4B and Table 1) (P = 0.5843, for eyesight and mouth; P = 0.3515, for eyesight and fingers). Note that a similar correlation existed between geometric dissimilarity and recall accuracy by eyesight (Fig. 6B). Unexpectedly, the recall accuracy of identical structures by eyesight was just 64.88% (Fig. 6B and Table 1), which is similar to accuracy values from oral and manual stereognosis. That is, eyesight seems to be no better than hand or mouth at identifying esoteric shapes.

Tiny tactile models

To our knowledge, the models tested here are the smallest molecular models ever fabricated and used by students. They can be visualized by hand or mouth. The millimeter-scale models we present are less expensive to make and easier to store and transport than conventional centimeter-scale models. The cost of 3D printer resin required to make the smaller microscale models is approximately $0.10 per model. In comparison, the cost of resin to produce a plum-sized model using our 3D printer is ~$5.00 per model. The high portability and low cost of microscale models can transform the way models are manufactured, presented, and studied by sighted or unsighted students. For example, ~100 smaller models can easily fit on a textbook-size page of cardboard paper, fixed with shrink-wrapping, and labeled with print or Braille. Identification of models with a smartphone-based machine learning application is also feasible, as each structure represents its own 3D quick response (QR) code (images in Fig. 1 were collected using a smartphone camera).

The methodology we describe is not limited to molecular models of protein structures. The high resolution of current 3D printers should enable fabrication of bite-size "ball and stick" models of small molecules, with rotatable or tortional bonds such as those presented in organic chemistry or introductory chemistry (e.g., butane, cyclohexane, and glucose). The methodology we describe is not limited to the field of chemistry but can involve models of any 3D image. For example, models of cellular organelles such as mitochondria are feasible, with quarter cross sections depicting tactile cristae, inner membranes, intermembrane space, and matrix.

Gelatin models were the only type of edible models that we tested. However, we were able to use silicone molds to produce high-resolution models from other edible materials, e.g., taffy and chocolate. Sticks could be grafted into edible models during fabrication (Fig. 7A).

Table 1. Recall accuracy of protein structures by oral tactile sensing (O), manual tactile sensing (M), and eyesight.

		No. of students	No. of tests	Recall accuracy ± SD	P value (t test)	Recall accuracy (of identical structures)	No. of students superior* (M)	No. of students superior (O)	No. of students equal (M=O)	P value (χ^2)
All models (college)[†]	Manual	281	4496	84.83 ± 15.14%	0.5477	68.25%	79	90	112	0.0491
	Oral			85.59 ± 14.65%		71.53%				
	Eyesight[‡]	84	672	87.50 ± 13.58%	0.5843[§]	64.88%	N/A	N/A	N/A	N/A
Small edible models (college)	Manual	32	512	81.25 ± 11.88%	0.7083	48.39%	11	12	9	0.8035
	Oral			80.08 ± 13.04%		51.61%				
Small nonedible models (college)	Manual	117	1872	91.03 ± 11.93%	0.5433	82.43%	32	24	61	<0.0001
	Oral			90.06 ± 12.23%		81.53%				
Smaller nonedible models (college)	Manual	132	2112	80.21 ± 16.49%	0.1699	60.98%	36	54	42	0.1482
	Oral			82.95 ± 15.9%		67.80%				
Small nonedible models (grade school)[ǁ]	Manual	31	186	79.57 ± 26.77%	0.7252	90.32%	5	4	22	<0.0001
	Oral			81.72 ± 20.80%		83.87%				
All models (college and grade school)	Manual	312	4682	84.31 ± 16.68%	0.4826	69.43%	84	94	134	0.0012
	Oral			85.21 ± 15.37%		72.19%				

*The number of students who scored highest in manual (M) or oral (O) stereognosis, or who scored equally in manual and oral stereognosis (M = O). †This entry includes all tests carried out on college students (i.e., tactile tests with small and smaller models, edible/nonedible, and tests with eyesight). ‡A physical model was not used for recognition tests by eyesight; rather, a large video image of the structure was used in each test. §Comparison of recognition by oral stereognosis and eyesight. ǁShort ("truncated") tests using fewer models were carried out on grade school/primary school students.

Information about the surface features of a model, for example, a protein's pattern of positive and negative surface charge, could be represented by painting patterns of flavor onto the model (Fig. 7B). Small nonedible models could be threaded with string or chain to form a necklace or bracelet for convenient handling and visualization (Fig. 7C).

Tiny tactile models will enable the serial visualization—by hand or mouth—of libraries of hundreds of different disposable models, by a single student (sighted or unsighted). Tiny models can make imagery more accessible to students throughout the course of their education. The appropriate age group for these models is the same age group to whom a picture would be shown. Our general goal at this point is simply to make the imagery of STEM accessible to students—to spark interest—whether or not the student understands the exact thing they are visualizing. The results of this study demonstrate that oral tactile visualization of noncognitive (esoteric) structures, such as molecular models, does not require prior training. Oral tactile sensing is certainly natural, per se, beginning as "rooting reflex" in neonates (56) and continuing in early childhood, possibly to assist in speech development (57).

The similar accuracies of eyesight and oral or manual sensing of models suggest that tiny models will be useful to students without visual impairments, as these students benefit from active learning with 3D models (58). The perception of ambiguous shapes (and confidence in perception) can be greater by manual tactile sensing than by eyesight (59). This effect might extend to oral tactile perception of ambiguous shapes.

Oral somatosensory perception of tiny models should be a useful addition to the repertoire of multisensory learning tools for students with extraordinary visual needs. Oral tactile sensors provide a new conduit for multisensory visualization of 3D systems. The tongue and lips should certainly not remain unused by students with BLV, in our opinion.

Science and blindness

Making science accessible to persons with blindness is a grand challenge. As we work to overcome this daunting challenge, we must remember that resolving blindness is what science does best. The business of science over the past century has been to help people visualize things they could never see with their eyes. A synthetic
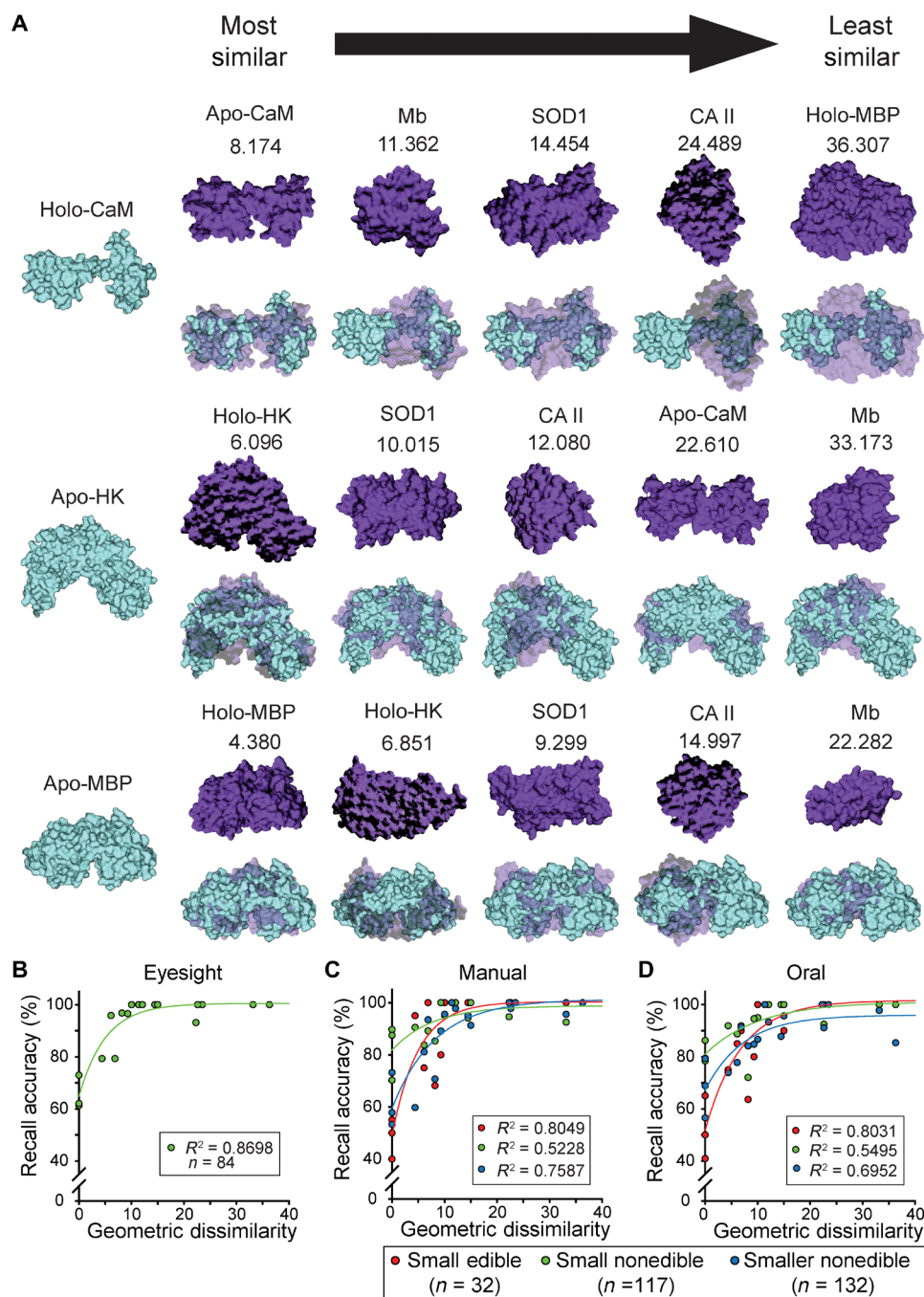
Fig. 6. Correlation between geometric similarity of structures and recall accuracy by mouth (oral tactile sensing), hand (manual tactile sensing), and eyesight. (**A**) Overlay of pairs of protein structures compared in this study and their geometric dissimilarity scores (smaller number = more similar). Structures in cyan are the study proteins that were given to students; structures in purple are test proteins. (**B** to **D**) Recall accuracy and geometric dissimilarity are exponentially related. Number of students tested: eyesight, $n = 84$ students; small edible models, $n = 32$ students; small nonedible models, $n = 117$; smaller nonedible models, $n = 132$.

chemist will never see the molecule that they labored so hard to build. The size of an atom is below the diffraction limit of visible light. Yet, the chemist still knows the position of each atom. They can recite the length and angle of every bond and can draw the structure of the molecule on a napkin. Scientists have worked around their blindness with cities full of assistive technology: x-ray diffractometers, mass spectrometers, nuclear magnetic resonance spectrometers, atomic force microscopes, and electron microscopes. This "science vision" is our heritage. It is grand and daunting too! This heritage dares us to create classrooms and laboratories and courses and research for anyone with a curious mind, regardless of their eyesight. It promises us that blindness is not a disqualifier from science. It is the beginning of science. It is an invitation to put on your goggles and come to laboratory.
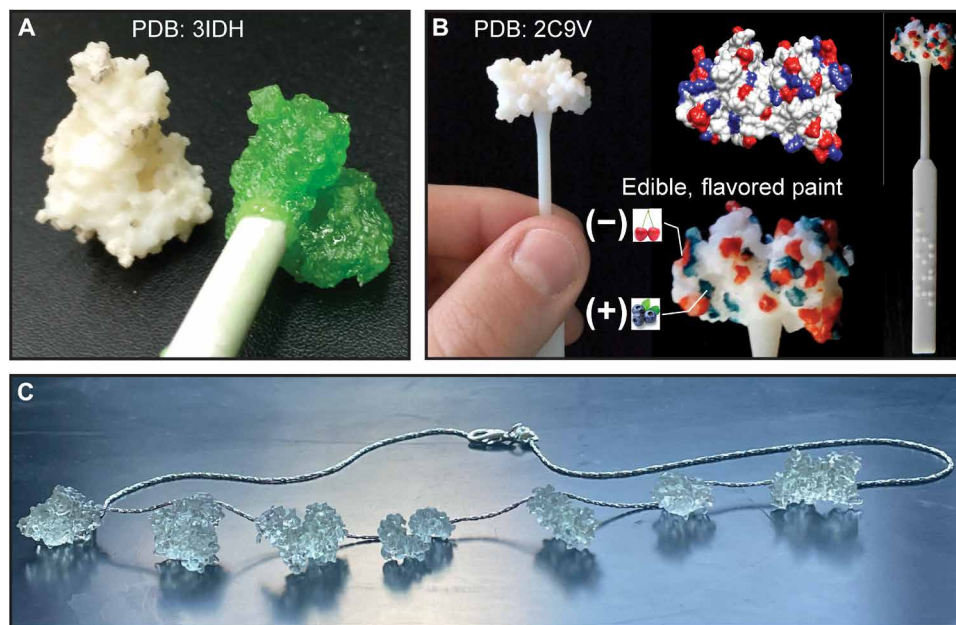
Fig. 7. Additional safety and functional features of tiny tactile models. (**A**) Gummy models (right) can be fabricated with lollipop sticks and remain similar in shape to nonedible model (left). This model is holo-HK (PDB code: 3DIH). (**B**) Nonedible models can have surface features, such as electrostatic surface potential, painted with flavored enamel. Here, the surface charge of SOD1 from the x-ray crystal structure is depicted on the model using red/cherry enamel (negative charge) and blue/blueberry enamel (positive charge). (**C**) Looping models together with chain or string represents a convenient method of packaging and handling. These models have peripheral eyelets; however, models could be printed with central bores for looping string/chain. Photo credit: Jordan C. Koone, Baylor University and Bryan F. Shaw, Baylor University.

MATERIALS AND METHODS
3D printing of nonedible models
3D printing occurred in a food-safe environment, using biocompatible, food-grade materials. Before use on human subjects, 3D-printed models were also autoclaved in a food-safe autoclave and stored in food-safe containers.

The 3D printing software PreForm (Formlabs) was used to create the layout of the printed proteins. The .STL file of each protein structure used was converted from the atomic coordinates of the following entries in the PDB: 1CFD (apo-CaM), 1OMP (MBP), 1V4T (apo-HK), 2C9V (SOD1), 3CLN (holo-CaM), 3IDH (substrate-bound HK), 3RGK (Mb), 4MBP (substrate-bound MBP), and 5A6H (CA).

Protein models were fabricated with a Formlabs printer, using surgical guide resin (an autoclavable, nontoxic, biocompatible resin). Small models were fabricated at a resolution of 100 μm, with a layer thickness of 0.1 mm. Smaller models were fabricated at a resolution of 50 μm, with a layer thickness of 0.05 mm. After models were printed, and individually taken off the build platform, they were hand-washed for 5 min in a bath of food-grade isopropyl alcohol. After washing, models were placed into the Form Wash and further rinsed with isopropyl alcohol for 20 min. After being washed, proteins were air-dried, and printing supports attached to the proteins were snapped off by gloved hand. The proteins were cured with ultraviolet light using the Form Cure apparatus (60°C for 30 min). After curing, the proteins were sterilized by autoclaving and stored in food-safe containers.

Fabrication of master silicone molds for edible models
Model templates, from which molds were made, were 3D-printed from .STL files of each protein structure. 3D-printed model templates were embedded in self-hardening clay (Amaco Marblex) along their longest axis, leaving approximately half of the model exposed. The clay was surrounded by an open-top box made of foam board and then covered with food-grade mold release spray. Food-grade silicone (Smooth-Sil 940) was prepared by mixing 600 ml of part A with at least 60 ml of part B. Silicone was then degassed (with the GoPlus New 2 Gallon Vacuum Changer and 3 CFM Single Stage Degassing Pump) and poured over the clay-embedded models approximately 30 min after spraying with mold release spray.

Immediately after the silicone was poured, any air bubbles that formed were removed with a toothpick. The silicone was allowed to cure at room temperature for 24 hours. This resulted in a compact block inside the foam board box composed of a clay half, a cured silicone half, and the 3D-printed models in-between the halves. The box was disassembled, and the clay was fully removed, leaving the 3D-printed models attached to the silicone half. The silicone mold containing 3D-printed models was encased in the same open box (with the 3D-printed models facing upwards) and sprayed with the same food-grade mold release. Degassed silicone was then poured over the cured silicone and models and allowed to cure. Once curing was complete, the two halves of the silicone mold were separated, and the 3D-printed models were removed from the molds. This process is illustrated in Fig. 2.

Preparation of gelatin
All edible models were prepared in a food-safe kitchen at the Mary Gibbs Jones Consumer Science Building at Baylor University. The gelatin gummy bear–like material that was injected into silicone molds was prepared from a combination of water, light corn syrup, unflavored gelatin powder (Knox Original Gelatin), and flavored "Jell-O" powder. Light corn syrup (30 mL) was added to 60 mL of

cold water, and the mixture was transferred to a large cooking pot. A full envelope (7 g) of unflavored gelatin was evenly spread across the liquid and allowed to swell until no powdered gelatin remained visible. Approximately 7.5 mL of flavored Jell-O powder was added to the mixture and stirred until homogeneous and then placed on an induction cook top and heated at a setting of 100 W (Mr. Induction SR964T Micro-Computer Induction Cooktop) for 2 min with continuous gentle stirring. After 2 min of cook time, the gelatin mixture was transferred to a wide-mouthed container (such as a measuring cup or drinking glass) so that any bubbles could rise to the top of the mixture and be removed easily. Once all air bubbles were removed, the mixture was promptly transferred to a fine-tipped confectioner's (decorating) bottle.

Injection of gelatin into silicone mold
Warm gelatin was injected into the silicone molds using the decorating bottle. Each half of the mold was filled with the liquid gelatin mixture and promptly pressed together into a single unit. Filled molds were placed in a refrigerator for 4 to 5 days to allow the gelatin mixture to harden. After refrigeration, the molds were separated, and excess gelatin was trimmed from around the filled cavities. The resulting edible models were left in one-half of the mold and allowed to dry at room temperature for another 2 days. This drying step is critical to preserve the shape of the model, as transferring the model to a flat surface before complete hardening can result in loss of shape during storage. After drying, models were carefully removed from mold and placed on parchment paper, with the half of the model previously exposed to air (i.e., the hardened side) facing downward. Models were left exposed for approximately 1 week to fully harden and were then stored in small plastic containers until use. Although edible models could be prepared with different flavors, we only tested subjects using a single flavor (typically, orange).

The production of edible gelatin models, from conversion of PDB file to creation of mold and finished model, was carried out by sighted students at Baylor University with no prior knowledge of 3D printing or silicone injection molding. Therefore, this methodology should be useable by any educator in any type of food-safe setting (classroom or kitchen). The food-grade materials required to fabricate molds, and gelatin models, are readily available from a grocery store, craft store, or online retailer. Although access to a 3D printer is required to produce the initial master model (from which the reusable silicone molds are fabricated), such printing can be performed by a third party for low cost. The number of edible models that can be made depends upon the number of master silicone injection molds that were prepared.

Selection of study participants
This study was approved by an Institutional Review Board at Baylor University. A total of 396 participants were tested. College-age students at Baylor University who, at the time of participation, were currently enrolled in organic chemistry or introductory biochemistry were given the opportunity to participate in this study. No students were excluded on any criteria, except for those wishing to participate with edible models who had dietary restrictions preventing them from consuming any ingredient of the gelatin mixture. Data from all students who participated in the study to completion are included. Elementary school–age students (fourth and fifth grade students) from a local grade school in Waco, Texas were also given the opportunity to participate with the same exclusion criteria (in addition to an age requirement of $\geq$7 years old). Informed consent, ascent, or parental consent was received from all participants. Of the 396 participants, 31 were fourth and fifth grade students and 365 participants were college students. Of the 365 college students, 59.5% of participants were female and 40.5% were male.

The visual acuity of students in this study was on the spectrum of normal, with a fraction wearing corrective lenses, but none needing accommodations. The only exception was a 10-year-old survivor of bilateral retinoblastoma (Fig. 5) who is visually impaired. This student underwent eye enucleation at 9 months old and has partial vision in his remaining eye (but was blindfolded during all tests). This student's test results (summarized in Fig. 5) are excluded from the aggregate dataset (but are included as an internal case study) because they were tested on a more extensive test format. However, we chose to include the results of their test because they were the first individual that this technology was tested upon, and for whom it was initially developed.

Testing protocols
All students (test subjects) in this study were blindfolded during testing of oral and manual tactile models, regardless of their visual acuity. Blindfolds were used not only to necessarily model complete vision loss but also to prevent students from seeing the models. Students who participated in the visual component of the research were not blindfolded. Individually wrapped "sleeping masks" were used as blindfolds. All test subjects (students) in this study (which ranged from fourth grade through college-age students) underwent similar testing procedures.

College-age participants were given a series of nine protein models, the first being the study protein and the remaining eight being the "test" proteins. Each student received either holo-CaM, apo-HK, or apo-MBP as their study protein. Apo and holo designations denoted different shapes and structures of the same molecule, induced by the binding of a metal ion or small organic molecule (i.e., carbohydrate). The remaining eight proteins included two instances of the study protein, two instances of the "opposite" conformation of their respective study protein (i.e., the apo- or holo-conformer), and four other structures including Mb, CA, SOD, and either apo-CaM, holo-HK, or holo-MBP. Test scores were calculated for each subject by dividing the number of correct answers by the total number of questions that were asked during tests. Elementary school age participants were given a series of only four proteins, one study protein (holo-CaM, apo-HK, or apo-MBP) followed by Mb, the study protein, and the opposite conformer of their study protein.

Regardless of age, each participant was given 3 min to assess/perceive/visualize the structure of their study protein with their fingertips followed by 1 min with each of the test proteins. After assessing each test protein, students were prompted to answer whether the protein was the same model or a different model than the initial study protein. The entire process was repeated using the oral cavity to discern shape instead of fingers. Here, students engaging in oral stereognosis were not allowed to touch the models with their hands. Instead, the model was placed in their mouth, or they were directed to pick up a lanyard attached to the model. Students who were asked to distinguish protein shapes with their eyesight were shown animations of each protein structure slowly spinning (so that they had a full 360° view of the structure). The size of the rotating molecular graphic was not reduced to the millimeter scale of the physical models but was kept at the standard centimeter scale

of a computer screen. The same test format (as the tactile tests) was used. Students were given 3 min to observe the study protein, followed by 1 min to assess each image of test proteins.

Students did not insert the models into their mouth by touching them, but either had them placed in their mouth by a researcher, picked up the model by the attached lanyard (without touching the actual model), or transferred them to their mouth via a pill box (without touching the model). Students were not instructed or advised on how to use their hands or mouth to tactilely sense the study model but simply asked to attempt to discern the shape with either oral or manual tactile sensing. Tests completed with eyesight were identical in format to the manual and oral tests. Rather than being given a 3D-printed model to visualize, the students were shown a presentation of animations of each protein structure spinning along the x and y axes.

Quantifying differences in shape of models

The geometric similarity of protein structures (i.e., topology) was quantified using CloudCompare (v2.10.2). Models were converted from .STL files to a surface mesh containing 1,000,000 points. From these points, the surface area, volume, and x, y, and z dimensions of the model were computed. Models were aligned, and the mesh-to-mesh distance was calculated on the registered pair. The maximum distance between two points was calculated. The similarity score is computed using Eq. 1. This score is expressed as the product of the maximum distance (D) between two points on the models, ratio of surface area (SA) of each model, ratio of volume of each model (V), and ratio of cubicity of each model ($x/y/z$) (C) (Eq. 1). Each contributing ratio was expressed to be ≥ 1, i.e., the larger value of each metric was placed in the numerator.

$$\text{Similarity} = D \cdot SA \cdot V \cdot C \tag{1}$$

SUPPLEMENTARY MATERIALS
Supplementary material for this article is available at http://advances.sciencemag.org/cgi/content/full/7/22/eabh0691/DC1

View/request a protocol for this paper from *Bio-protocol*.

REFERENCES AND NOTES

1. R. R. A. Bourne, S. R. Flaxman, T. Braithwaite, M. V. Cicinelli, A. Das, J. B. Jonas, J. Keeffe, J. H. Kempen, J. Leasher, H. Limburg, K. Naidoo, K. Pesudovs, S. Resnikoff, A. Silvester, G. A. Stevens, N. Tahhan, T. Y. Wong, H. R. Taylor; Vision Loss Expert Group, Magnitude, temporal trends, and projections of the global prevalence of blindness and distance and near vision impairment: A systematic review and meta-analysis. *Lancet Glob. Health* **5**, e888–e897 (2017).
2. G. Parikshit, G. Clare, Blindness in children: A worldwide perspective. *Community Eye Health* **20**, 32–33 (2007).
3. National Science Foundation, Employed scientists and engineers, by occupation, highest degree level, and disability status: 2017 (2017); https://ncses.nsf.gov/pubs/nsf19304/data.
4. J. T. E. Richardson, Academic attainment in visually impaired students in distance education. *Br. J. Vis. Impair.* **33**, 126–137 (2015).
5. T. Wild, A. Allen, Policy analysis of science-based best practices for students with visual impairments. *J. Vis. Impair. Blind.* **103**, 113–117 (2009).
6. I. Singhal, B. S. Balaji, Creating atom representations using open-source, stackable 3D printed interlocking pieces with tactile features to support chemical equation writing for sighted and visually impaired students. *J. Chem. Educ.* **97**, 118–124 (2020).
7. C. A. Supalo, M. D. Isaacson, M. V. Lombardi, Making hands-on science learning accessible for students who are blind or have low vision. *J. Chem. Educ.* **91**, 195–199 (2014).
8. G. M. Nepomuceno, D. M. Decker, J. D. Shaw, L. Boyes, D. J. Tantillo, H. B. Wedler, The value of safety and practicality: Recommendations for training disabled students in the sciences with a focus on blind and visually impaired students in chemistry laboratories. *J. Chem. Health Saf.* **23**, 5–11 (2016).
9. A. J. Hoffman, L. McGuire, A. Rutland, A. Hartstone-Rose, M. J. Irvin, M. Winterbottom, F. Balkwill, G. E. Fields, K. L. Mulvey, The relations and role of social competencies and belonging with math and science interest and efficacy for adolescents in informal STEM programs. *J. Youth Adolesc.* **50**, 314–323 (2021).
10. U. Tellhed, M. Bäckström, F. Björklund, Will I fit in and do well? The importance of social belongingness and self-efficacy for explaining gender differences in interest in STEM and HEED Majors. *Sex Roles* **77**, 86–96 (2017).
11. B. Ertl, F. G. Hartmann, The interest profiles and interest congruence of male and female students in STEM and non-STEM fields. *Front. Psychol.* **10**, 897 (2019).
12. Z. Hazari, G. Potvin, J. D. Cribbs, A. Godwin, T. D. Scott, L. Klotz, Interest in STEM is contagious for students in biology, chemistry, and physics classes. *Sci. Adv.* **3**, e1700046 (2017).
13. T. Bualar, Barriers to inclusive higher education in Thailand: Voices of blind students. *Asia Pac. Educ. Rev.* **19**, 469–477 (2018).
14. I. F. W. K. Davidson, J. N. Simmons, Mediating the environment for young blind-children: A conceptualization. *J. Vis. Impair. Blind.* **78**, 251–255 (1984).
15. G. A. Fernandez, R. A. Ocampo, A. R. Costantino, N. S. Dop, Application of didactic strategies as multisensory teaching tools in organic chemistry practices for students with visual disabilities. *J. Chem. Educ.* **96**, 691–696 (2019).
16. W. J. Fraser, M. O. Maguvhe, Teaching life sciences to blind and visually impaired learners. *J. Biol. Educ.* **42**, 84–89 (2008).
17. B. Anđić, S. Cvjetićanin, M. Maričić, D. Stešević, Sensory perception and descriptions of morphological characteristic of vegetative plant organs by the blind: Implementation in teaching. *J. Biol. Educ.*, 1–19 (2019).
18. N. N. Stepien-Bernabe, D. Lei, A. McKerracher, D. Orel-Bixler, The impact of presentation mode and technology on reading comprehension among blind and sighted individuals. *Optom. Vis. Sci.* **96**, 354–361 (2019).
19. C. M. Graybill, C. A. Supalo, T. E. Mallouk, C. Amorosi, L. Rankel, Low-cost laboratory adaptations for precollege students who are blind or visually impaired. *J. Chem. Educ.* **85**, 243–247 (2008).
20. S. M. Weisberg, N. S. Newcombe, Embodied cognition and STEM learning: Overview of a topical collection in CR:PI. *Cogn. Res. Princ. Implic.* **2**, 38 (2017).
21. D. DeSutter, M. Stieff, Teaching students to think spatially through embodied actions: Design principles for learning environments in science, technology, engineering, and mathematics. *Cogn. Res. Princ. Implic.* **2**, 22 (2017).
22. L. P. Rosenblum, L. Cheng, C. R. Beal, Teachers of students with visual impairments share experiences and advice for supporting students in understanding graphics. *J. Vis. Impair. Blind.* **112**, 475–487 (2018).
23. D. L. Nelson, M. M. Cox, *Lehninger Principles of Biochemistry* (W. H. Freeman, ed. 7, 2017).
24. H. B. Wedler, S. R. Cohen, R. L. Davis, J. G. Harrison, M. R. Siebert, D. Willenbring, C. S. Hamann, J. T. Shaw, D. J. Tantillo, Applied computational chemistry for the blind and visually impaired. *J. Chem. Educ.* **89**, 1400–1404 (2012).
25. R. Jacobs, C. Bou Serhal, D. van Steenberghe, Oral stereognosis: A review of the literature. *Clin. Oral Investig.* **2**, 3–10 (1998).
26. R. Fujii, T. Takahashi, A. Toyomura, T. Miyamoto, T. Ueno, A. Yokoyama, Comparison of cerebral activation involved in oral and manual stereognosis. *J. Clin. Neurosci.* **18**, 1520–1523 (2011).
27. P. D. Howes, S. Wongsriruksa, Z. Laughlin, H. J. Witchel, M. Miodownik, The perception of materials through oral sensation. *PLOS ONE* **9**, e105035 (2014).
28. P. Haggard, L. de Boer, Oral somatosensory awareness. *Neurosci. Biobehav. Rev.* **47**, 469–484 (2014).
29. D.-R. Chebat, C. Rainville, R. Kupers, M. Ptito, Tactile-'visual' acuity of the tongue in early blind individuals. *Neuroreport* **18**, 1901–1904 (2007).
30. B. L. Miles, K. Van Simaeys, M. Whitecotton, C. T. Simons, Comparative tactile sensitivity of the fingertip and apical tongue using complex and pure tactile tasks. *Physiol. Behav.* **194**, 515–521 (2018).
31. R. W. Van Boven, K. O. Johnson, The limit of tactile spatial resolution in humans: Grating orientation discrimination at the lip, tongue, and finger. *Neurology* **44**, 2361–2366 (1994).
32. B. L. Miles, S. L. Ang, C. T. Simons, Development of a "pure-tactile" assessment of edge discrimination in the hands and oral cavity. *Physiol. Behav.* **224**, 113035 (2020).
33. B. Linne, C. T. Simons, Quantification of oral roughness perception and comparison with mechanism of astringency perception. *Chem. Senses* **42**, 525–535 (2017).
34. B. F. Shaw, Oral-based method and system for educating visually impaired students. U.S. Patent 10,043,413 B2 (2018).
35. J. J. Miyamoto, M. Honda, D. N. Saito, T. Okada, T. Ono, K. Ohyama, N. Sadato, The representation of the human oral area in the somatosensory cortex: A functional MRI study. *Cereb. Cortex* **16**, 669–675 (2006).
36. Y. Tamura, Y. Shibukawa, M. Shintani, Y. Kaneko, T. Ichinohe, Oral structure representation in human somatosensory cortex. *Neuroimage* **43**, 128–135 (2008).
37. L. Mu, I. Sanders, Human tongue neuroanatomy: Nerve supply and motor endplates. *Clin. Anat.* **23**, 777–791 (2010).

38. P. Stål, S. Marklund, L.-E. Thornell, R. De Paul, P.-O. Eriksson, Fibre composition of human intrinsic tongue muscles. *Cells Tissues Organs* **173**, 147–161 (2003).

39. W. M. Kier, K. K. Smith, Tongues, tentacles and trunks: The biomechanics of movement in muscular-hydrostats. *Zool. J. Linn. Soc.* **83**, 307–324 (1985).

40. L. Engelen, J. F. Prinz, F. Bosman, The influence of density and material on oral perception of ball size with and without palatal coverage. *Arch. Oral Biol.* **47**, 197–201 (2002).

41. K. Drewing, The extent of skin bending rather than action possibilities explains why holes feel larger with the tongue than with the finger. *J. Exp. Psychol. Hum. Percept. Perform.* **44**, 535–550 (2018).

42. M. Wong, V. Gnanakumaran, D. Goldreich, Tactile spatial acuity enhancement in blindness: Evidence for experience-dependent mechanisms. *J. Neurosci.* **31**, 7028–7037 (2011).

43. R. W. Van Boven, R. H. Hamilton, T. Kauffman, J. P. Keenan, A. Pascual-Leone, Tactile spatial resolution in blind braille readers. *Neurology* **54**, 2230–2236 (2000).

44. G. E. Legge, C. Madison, B. N. Vaughn, A. M. Y. Cheong, J. C. Miller, Retention of high tactile acuity throughout the life span in blindness. *Percept. Psychophys.* **70**, 1471–1488 (2008).

45. J. F. Norman, A. N. Bartholomew, Blindness enhances tactile acuity and haptic 3-D shape discrimination. *Atten. Percept. Psychophys.* **73**, 2323–2331 (2011).

46. J. C. Stevens, E. Foulke, M. Q. Patterson, Tactile acuity, aging, and braille reading in long-term blindness. *J. Exp. Psychol. Appl.* **2**, 91–106 (1996).

47. D. Goldreich, I. M. Kanics, Tactile acuity is enhanced in blindness. *J. Neurosci.* **23**, 3439–3445 (2003).

48. F. Alary, M. Duquette, R. Goldstein, C. E. Chapman, P. Voss, V. La Buissonnière-Ariza, F. Lepore, Tactile acuity in the blind: A closer look reveals superiority over the sighted in some but not all cutaneous tasks. *Neuropsychologia* **47**, 2037–2043 (2009).

49. A. C. Grant, M. C. Thiagarajah, K. Sathian, Tactile perception in blind Braille readers: A psychophysical study of acuity and hyperacuity using gratings and dot patterns. *Percept. Psychophys.* **62**, 301–312 (2000).

50. H. R. Dinse, N. Kleibel, T. Kalisch, P. Ragert, C. Wilimzig, M. Tegenthoff, Tactile coactivation resets age-related decline of human tactile discrimination. *Ann. Neurol.* **60**, 88–94 (2006).

51. F. Vega-Bermudez, K. O. Johnson, Fingertip skin conformance accounts, in part, for differences in tactile spatial acuity in young subjects, but not for the decline in spatial acuity with aging. *Percept. Psychophys.* **66**, 60–67 (2004).

52. P. Ragert, A. Schmidt, E. Altenmüller, H. R. Dinse, Superior tactile performance and learning in professional pianists: Evidence for meta-plasticity in musicians. *Eur. J. Neurosci.* **19**, 473–478 (2004).

53. D. Bracken-Roche, E. Bell, M. E. Macdonald, E. Racine, The concept of 'vulnerability' in research ethics: An in-depth analysis of policies and guidelines. *Health Res. Pol. Syst.* **15**, 8 (2017).

54. M. Wong, E. Hackeman, C. Hurd, D. Goldreich, Short-term visual deprivation does not enhance passive tactile spatial acuity. *PLOS ONE* **6**, e25277 (2011).

55. R. G. Bangcuyo, C. T. Simons, Lingual tactile sensitivity: Effect of age group, sex, and fungiform papillae density. *Exp. Brain Res.* **235**, 2679–2688 (2017).

56. K. R. Glodowski, R. H. Thompson, L. Martel, The rooting reflex as an infant feeding cue. *J. Appl. Behav. Anal.* **52**, 17–27 (2019).

57. M. Zuccarini, A. Guarini, J. M. Iverson, E. Benassi, S. Savini, R. Alessandroni, G. Faldella, A. Sansavini, Does early object exploration support gesture and language development in extremely preterm infants and full-term infants? *J. Commun. Disord.* **76**, 91–100 (2018).

58. D. L. Newman, D. Stefkovich, C. Clasen, M. A. Franzen, L. K. Wright, Physical models can provide superior learning opportunities beyond the benefits of active engagements. *Biochem. Mol. Biol. Educ.* **46**, 435–444 (2018).

59. M. T. Fairhurst, E. Travers, V. Hayward, O. Deroy, Confidence is higher in touch than in vision in cases of perceptual ambiguity. *Sci. Rep.* **8**, 15604 (2018).

Citation: K. M. Baumer, J. J. Lopez, S. V. Naidu, S. Rajendran, M. A. Iglesias, K. M. Carleton, C. J. Eisenmann, L. R. Carter, B. F. Shaw, Visualizing 3D imagery by mouth using candy-like models. *Sci. Adv.* **7**, eabh0691 (2021).